Combining plasmonic trap filling and optical backscattering for highly efficient third generation solar cells

Chen Wang,[†] Chang Li,[†] Shanpeng Wen,[,†] Pengfei Ma,[†] Yang Liu,[‡] Roderick C. I. MacKenzie,[*,§] Wenjing Tian,[‡] and Shengping Ruan[†]*

[†]State Key Laboratory on Integrated Optoelectronics and College of Electronic Science & Engineering, Jilin University, Changchun 130012, P. R. China. [*]E-mail: sp_wen@jlu.edu.cn

[‡]State Key Laboratory of Supramolecular Structure and Materials, Jilin University, Changchun 130012, P. R. China.

[§]University of Nottingham, University Park, Nottingham, NG7 2RD, UK. [*]E-mail: Roderick.Mackenzie@nottingham.ac.uk

ABSTRACT

Metal oxide contact layers such as ZnO and TiOx are commonly used in third generation solar cells as they can be solution processed and have a relatively high conductivity. It is well known, that by ultraviolet (UV) light soaking such devices overall device efficiency can be boosted. This improvement in efficiency is due to high energy UV light exciting hot carriers which then fill trap states in the metal oxide film. Unfortunately, UV causes degradation of the active layer and thus must be filtered out if long lifetimes are to be achieved. In this work, it is demonstrated that plasmonically excited metal nano-structures embedded in the ZnO metal oxide layer can generate hot charge carriers from visible light alone, thus removing the need for UV light soaking. Furthermore, using this approach the solar cells exhibit simultaneously improved charge transport/recombination properties as well as enhanced light trapping behavior. Consequently, the power conversion efficiency of a low-bandgap thieno[3,4-b]thiophene/benzodithiophene (PTB7) based solar cell can be increased from 7.91% to 9.36%.

KEYWORDS: metal oxides, plasmonic nanostructures, hot carriers, trap filling, organic solar cells

INTRODUCTION

Plasmonic nanostructures such as metallic nanoparticles (MNPs) have recently attracted considerable interest for their ability to support localized surface plasmon resonances (LSPR).[1-3] By exploiting size-function relationships the optical properties of the nanoparticles can be easily tuned,[4-6] making them suitable for optoelectronic applications such as photo-detectors[7] and solar cells.[8,9] In particular, the highly confined LSPR modes provide a feasible strategy for bulk heterojunction (BHJ) organic solar cells (OSCs) to achieve better optical absorption without increasing the thickness of organic layer.[10] It is well known that when integrated into OSCs, these metal nano-particles can act as sub-wavelength antennas facilitating near-field electromagnetic-field concentration or light scattering centres by far-field photon re-emission,[11-13] consequently they enable more light to be trapped inside the active layer and enhancing its absorption.

Furthermore, it has been demonstrated that properly designed MNPs can also convert incident photons directly into charge carriers.[14-16] The first report of this was by Zhao et al., they observed an anodic photocurrent when illuminating a bi-layer of TiO_2-film/gold (or silver) nanoparticles with green light.[17] This phenomenon was later attributed to plasmon-induced hot-electrons formation.[18] Key to this process is fast charge transfer between the nano-particles and the semiconductor to avoid recombination/relaxation events. N-type metal-oxides such as ZnO and TiO_x have been shown to permit fast charge transfer.[19-21] In addition, these N-type metal-oxides are also regarded as very attractive materials for the electron transport layer (ETL) in solar cells.[22,23] However, one drawback of using these materials for the ETL is that they have many structural defects, such as Zn/Ti/oxygen vacancies, and therefore have many mid-gap trap states, which through recombination reduce overall cell efficiency.[24-27] It has been reported that

continuous UV light soaking[28,29] can help fill states and result in enhanced device performance. However, using UV light has the drawback of damaging the device and prematurely degrading the active layer, which is incompatible with the search for long lifetime third generation solar cells.[30] A more attractive approach would be to plasmonically sensitize the metal-oxide layer, by embedding metal nano-particles within the ETL matrix. This would enable hot charge carriers to be generated from low energy visible light, which would then be able to fill defect states and eliminate the need for UV light soaking.

Recently Choy et al. demonstrated that by embedding gold (Au) nanospheres within a TiO_2 matrix, charge carrier trap states could be filled, and the overall electrical properties of the film could be improved.[31] However, when this material system was used as the ETL in an organic solar cell, only a modest increase in cell efficiency was observed. This was probably because spherical nano-particles are not an optimal shape for electric field enhancement.[32] Furthermore, these nanospheres only measured 15 nm wide which reduced their ability to scatter light.[33] Embedding proper nano-particles into ETL to combine hot-electron generation and also light scattering effect thus would be attractive. But the confirmed relationship between the preferred effect and nano-particle size[33,34] requires the selected nano-particles should be adjustable on multiple dimensions. Sphere's isotropy determines that it has only one dimension to regulate. By contrast, anisotropic nanorods provide two dimensions that can be tuned, so as to act as light scattering centers[2,35] as well as active elements for hot-electron generation.[36,37]

So in this work, we synthesize anisotropic Au nanorods (AuNRs) to embed in ZnO transport layer; these NRs exhibit a highly localized electric-field stemming from the longitudinal resonance mode. Furthermore, the short sides of NRs can easily be tuned to meet the requirements of hot-electron generation from visible light. Meanwhile, the long sides of NRs can

offer sufficient cross-section area for light scattering. This provides a good platform for improving electrical properties of ZnO without sacrificing its light scattering effects. We found that after soaking the cells with visible light overlapping the plasmon resonance energy of the nanorods, the cells exhibited higher average mobility values and lower charge carrier recombination rates. We attribute this to better charge extraction through the modified ZnO transport layer. This lead to a boost in efficiency from 7.91% to 9.36%. Thus, we present a general strategy, for ETL design which improves both the electrical and optical properties of third generation solar cells.

RESULTS AND DISCUSSION

Figure 1 depicts, the device structure, chemical structure of organic materials and transmission electron microscopy (TEM) images of nanoparticles. The synthesis of the nanoparticles is described in the Supporting Information. High-resolution TEM (HR-TEM) analysis showed that the ZnO nano-particles had a diameter of around 5 nm, while the as-prepared AuNRs exhibited relatively uniform shapes with an average length of 50 nm and diameter of 20 nm. Corresponding transverse and longitudinal plasmon resonance peaks were located at 515 nm and 691 nm, respectively (Figure S1). It has previously been reported[35,36,40,41] that light scattering is the dominant process in large plasmonic nanostructures (>50 nm) while the non-radiative decay of plasmons via the emission of hot charge carrier to the neighboring semiconductor can dominate in small nanostructures (<30 nm). Therefore by tuning one side of the NP to be ~50 nm it will be able to scatter light efficiently, while the shorter side will be able to assist in hot carrier generation. AuNRs colloid (0-4% wt) was mixed with ZnO solution before being spin-coated onto a PTB7:$PC_{71}BM$ layer to form $\approx$ 35 nm thick ZnO/AuNRs composite film.

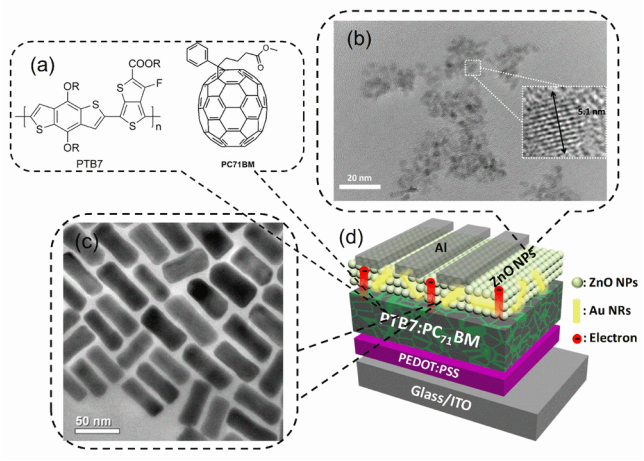

Figure 1. (a): the chemical structure of PTB7 and $PC_{71}BM$; (b): HR-TEM images of ZnO NPs, the inset shows the size of ZnO NPs; (c): HR-TEM images of as-prepared AuNRs; (d): the ITO(150nm)/PEDOT:PSS(40 nm)/PTB7:$PC_{71}BM$(95 nm) /ZnO(AuNRs) (35 nm)/Al (100 nm) device.

Figure 2, depicts an AFM image of a ZnO film with and without AuNRs, it can be seen that there is little change in the morphology due to the addition of the AuNRs. Root-mean-squared (RMS) surface roughness of the film slightly increased upon addition of the nanorods from 2.24 nm to 2.86 nm, which suggests that incorporating AuNRs has minimal influence on the formation of ZnO layer and guarantees its interfacial properties as optical spacer.

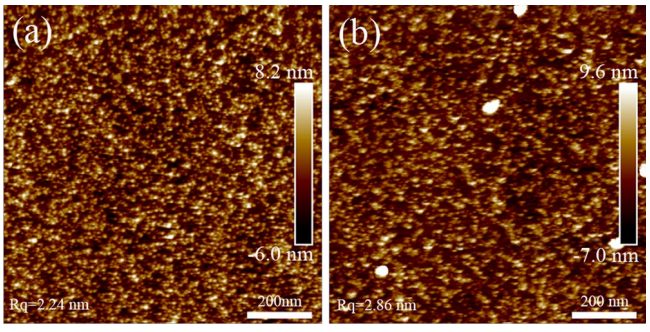

Figure 2. The AFM height images of ZnO film without (a) and with (b) AuNRs.

To characterize the ZnO/AuNRs layer, we performed photoluminescence (PL) measurements to confirm that the AuNRs can generate hot charge carriers after surface plasmon excitation which will in turn fill the ZnO trap states. Figure 3a shows the PL spectrum produced by exciting a pure ZnO film with a 350 nm source, while Figure 3b, shows the PL spectrum produced after exciting a ZnO film with embedded AuNRs. In both Figure 3a and 3b, one curve is shown where the sample was not light soaked before the measurement, and one curve where the sample was light soaked with visible light containing no UV component. For the neat ZnO film (Figure 3a), a broad band emission with maximum at 527 nm can be seen, which is ascribed to defect emission owing to the low processing temperature of our ZnO NPs. This can be attributed to a mid-gap trap level at -5.32 eV that corresponds to the singly ionized oxygen vacancy (V^+).[40] The introduction of AuNRs (2% wt) into ZnO layer didn't significantly change the emission level. Both samples were then placed under solar irradiation ($\lambda > 410$ nm) for 5 min as pre-illumination. It can be seen from Figure 3b (red line) that, the defect emission of the composite film was effectively quenched after plasmon excitation. While same treatment for neat ZnO film didn't lead to the reduction of PL intensity. This behavior verified that the LSPR-excited AuNRs encouraged the trap filling in ZnO without the aid of UV light.

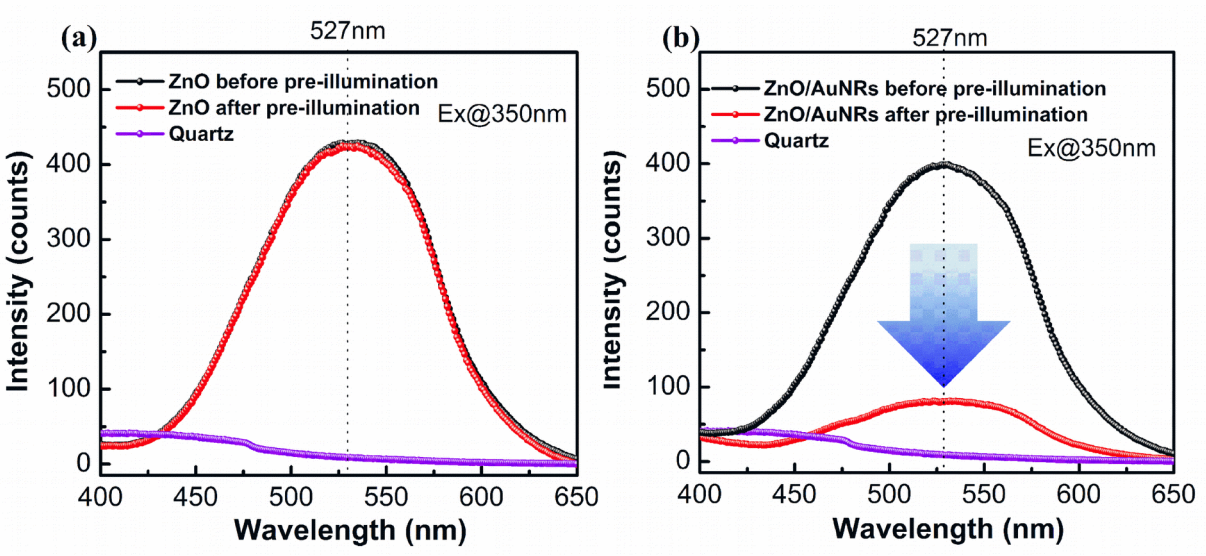

Figure 3. Photoluminescence (PL) spectra of ZnO film without (a) and with (b) AuNRs before (black) and after (red) pre-treatment.

We then fabricated two types of solar cells, one with pure ZnO as the ETL (denote as reference device) and one with ZnO embedded with AuNRs (denote as plasmonic device). Figure 4 plots the current density-voltage (*J*-*V*) curves produced by the cells under AM 1.5 G illuminations. Before recording the *J*-*V* curves, the cells were placed in front of the aforementioned solar simulation (with no UV component). It can be seen that the maximum power conversion efficiency (PCE) of reference devices was 7.91% with an open-circuit voltage (V_{oc}) of 0.741 V, a short-circuit current density (J_{sc}) of 16.36 mA cm-2 and a fill factor (FF) of 65.2%, which is comparable to those of previously reported works based on PTB7:$PC_{71}BM$.[41] More detailed statistical performance parameters can be found in Table 1. It can be seen that the plasmonic devices exhibited better performances. The optimal concentration of AuNRs was 2% wt. The best performance was mainly improved by the increase in J_{sc} from 16.36 to 17.76 mA cm^{-2} and the FF from 64.2% to 70.5% respectively. The V_{oc} was only slightly improved. As a result, a PCE

of 9.36% was obtained by the champion device. This is among the highest efficiencies reported for the PTB7:$PC_{71}BM$ system.[42-44] By measuring 10 optimized devices, we obtained the following figures of merit: V_{oc} at 0.742±0.004 V, J_{sc} at 17.73±0.22 mA cm^{-2}, FF at 69.8±0.5% and PCE at 9.18±0.13%. We noted that when the AuNRs concentration was further increased to 4%, the cell efficiency decreased. Our experiments indicate that excess AuNRs may act as recombination centers[45] that decrease the charge carrier lifetime and extraction efficiency (vide infra). Quantum efficiency of device containing 4% AuNRs was plotted in SI (see Fig. S2), this shows the 4% device also has a lower EQE across the entire spectrum, supporting the fact that the decrease in efficiency is due to an electrical effect. It is also worth noting that even without the light soaking, the plasmonic device performance was improved, but only by a modest amount mainly due to a slightly improved photocurrent. We attribute this to the enhanced light absorption induced by LSPR effect.

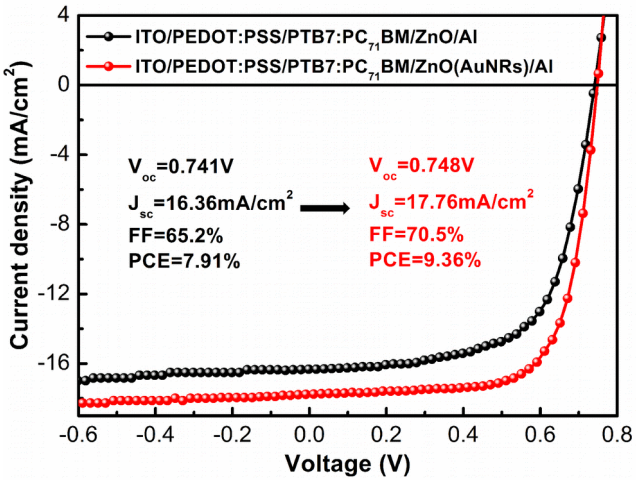

Figure 4. The *J-V* characteristics of the OSCs using ZnO and ZnO/AuNRs as ETL without and with AuNRs.

Table 1. *J-V* performance parameters of the OSCs without and with different concentration AuNRs.

AuNRs concentration	Pre-illumination	V_{oc} (V)	J_{sc} (mA cm^{-2})	FF (%)	PCE (%)
0% wt	yes	0.738±0.002	16.40±0.37	64.1±0.9	7.76±0.14 (7.91)[a)]
1% wt	yes	0.740±0.002	17.22±0.23	68.6±0.4	8.74±0.13 (8.89)
2% wt	yes	0.742±0.004	17.73±0.22	69.8±0.5	9.18±0.13 (9.36)
4% wt	yes	0.738±0.003	17.29±0.29	68.1±0.3	8.69±0.12 (8.80)
0% wt	no	0.737±0.002	16.53±0.25	64.7±0.5	7.89±0.09 (8.05)
2% wt	no	0.738±0.002	17.36±0.16	65.0±1.0	8.37±0.08 (8.48)

[a)]The value in brackets is the best PCE for each device.

In order to obtain a more comprehensive understanding of the photocurrent enhancement, we measured the external quantum efficiency (EQE) from the devices, as shown in Figure 5. It can be seen that the EQE was uniformly enhanced over a broad spectral region from 350 to 700 nm with a maximum EQE value for the plasmonic device up to 78%. EQE-integrated J_{sc}s for these devices were comparable to the actual measured J_{sc}s, further confirming our observation. As the EQE enhancement is broad and uniform, this implies that the ZnO/AuNRs composite ETL improved the electrical performance of solar cells, one if the improvement were mainly due to optical effects a more wavelength depended change in the EQE spectra would be expected. The significantly higher FF of 69.8±0.5% of plasmonic devices also suggests efficient charge transport and suppressed carrier recombination in the cells, which is consistent with better charge carrier extraction properties.

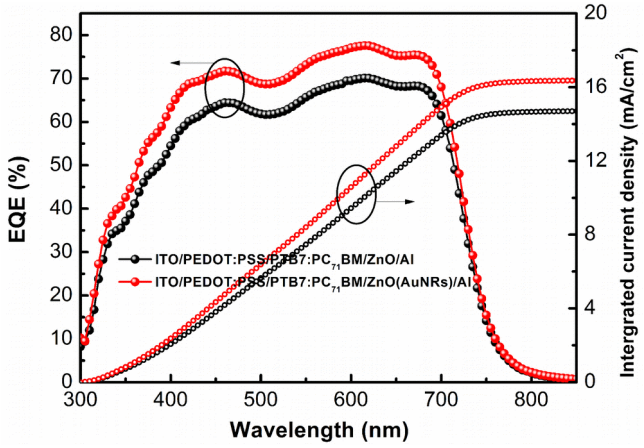

Figure 5. The EQE response spectra of reference and plasmonic devices.

To study how plasmonic enhancement affected over all device mobility, we used the space charge limited current (SCLC) method to investigate three types of devices; a) hole-only devices (ITO/PEDOT:PSS/PTB7:$PC_{71}BM$/Au); b) electron-only devices with a pure ZnO ETL (ITO/TiO_x/PTB7:$PC_{71}BM$/ZnO/Al); and c) electron-only devices with a ZnO/AuNRs ETL (ITO/TiO_x/PTB7:$PC_{71}BM$/ZnO/Al). The results are plotted in Figure 6. Note all devices reported in this section were light soaked before being measured.

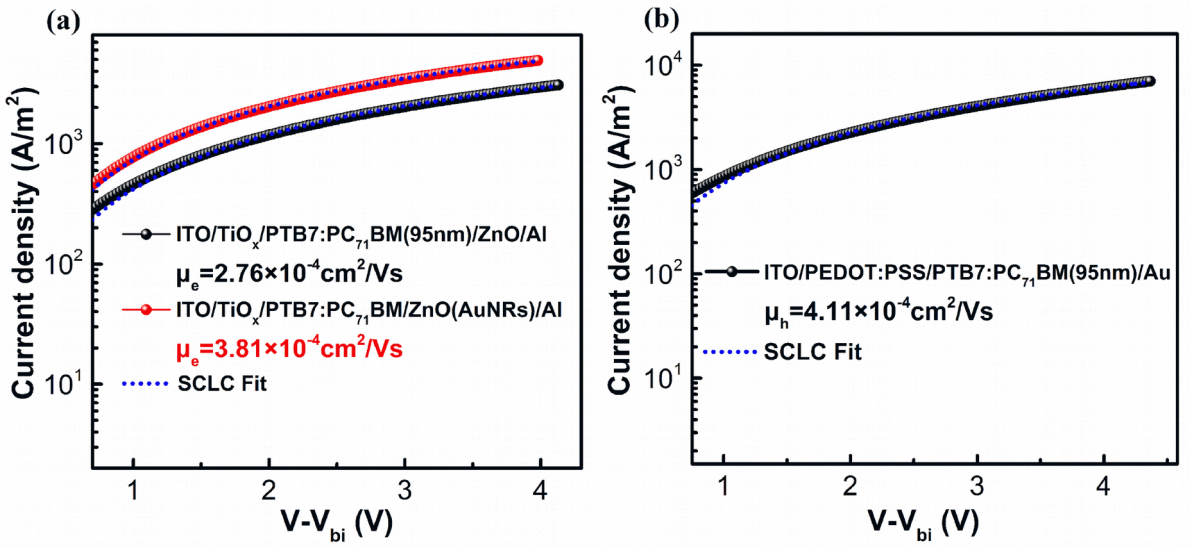

Figure 6. Dark *J-V* characteristics of electron-only devices (a) and hole-only devices (b). Where V is the applied voltage and V_{bi} is the built in voltage. V_{bi} accounts from the difference in work functions between the contact materials and was calculated from the threshold voltage of the diode. V_{bi} was measured at 0.64 V for the hole only device, 0.87 V and 1.02 V for the electron only device using ZnO and ZnO(2wt% AuNRs) as interfacial layer, respectively.

From Figure 6a, it can be seen that ZnO/AuNRs devices exhibit a higher electron current density than their pure ZnO counterparts, suggesting that the presence of AuNRs aids electron extraction. We calculated a corresponding increase in average device mobility from 2.76×10^{-4} cm^2/Vs to 3.81×10^{-4} cm^2/Vs. From Figure 6b, the hole mobility is calculated to be 4.11×10^{-4} cm^2/Vs, this is in agreement with previously reported values.[46] These results suggest that, carrier transport inside the devices became more balanced upon the inclusion of the AuNRs and thus reduced the effect of space charge that usually adversely affects the electrical performance of the device.[47] We take the view that the improved charge transport and extraction can be attributed to the plasmonically excited hot-electrons in AuNRs filling the trap states in ZnO and improving its mobility.

Measuring mobility in disordered materials is notoriously difficult, as the mobility changes as a function of carrier density, and hence as a function of measurement conditions. Different measurement techniques are also known to produce different values of mobility. Therefore, to check that the ZnO/AuNRs device really does have better charge transport properties and to aid comparison with previously published experimental data we perform Transient Photo Current (TPC) measurements. Figure 7 shows the normalized TPC transients from devices with a ZnO ETL, a ZnO/AuNRs ETL and a device with no ETL. It can be seen that in all cases a typical TPC

trace is observed, which is characterized by an initial plateau where charge transport dominates the transient and trap states are filled, followed by a sloped region, which is dominated by charge carrier detrapping from trap states.[48] It is noticeable that the plasmonic device had a shorter pre-transit period than the other two non-plasmonic devices, we attribute this to better charge carrier extraction from the device. We estimate the charge carrier mobility using equation

$$\mu = d^2 / \tau_i V$$

where d is active layer thickness, τ_i is transit time and V is the build-in voltage. The transit time (τ_i) was found to be 1.37, 1.26 and 1.09 μs for bare Al, ZnO/Al and ZnO(AuNRs)/Al, respectively. ZnO/AuNRs based cells had highest carrier mobility, giving a value of 1.06×10^{-4} cm^2/Vs. We again attribute this to free carriers being able to leave the device more quickly when trap states in ZnO have been filled by plasmonically generated charge carriers.

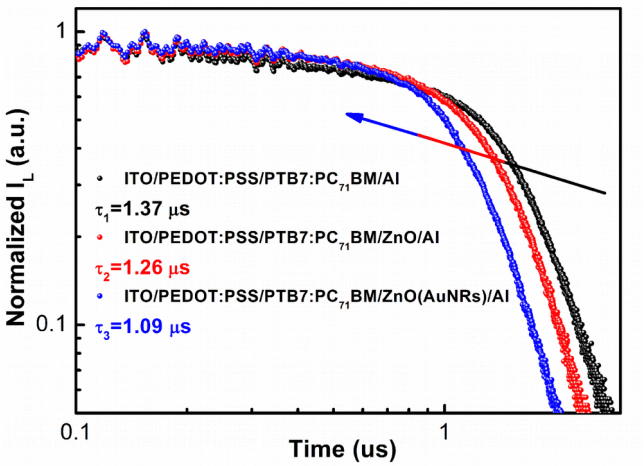

Figure 7. The normalized TPC curves of three types of PTB7-based solar cells.

Next, to examine how the addition of the AuNRs affected charge carrier recombination in the device, we performed photoinduced charge carrier extraction by linearly increasing voltage (photo-CELIV) measurements (see Fig. S4 in the SI).[49,50] In the photo-CELIV experiment, an

optical pulse is applied to a device, then at time t_{delay} after the pulse the charge carriers are extracted by applying a linearly increasing negative voltage transient. By varying t_{delay} the decay rate of photoexcited charge carriers can be studied.

Figure 8 plots the photoexcited charge extracted from the device as a function of t_{delay}. We fit this curve with the carrier recombination dynamic model[51] expressed by the equation

$$n(t) = \frac{n(0)}{1 + \left(\frac{t}{\tau}\right)^{\gamma}}$$

in which $n(0)$ is initial photo-generated carrier density and τ is carrier recombination lifetime. We estimated $n(0)$ to be 9.78×10^{15} cm^{-3} for the ZnO device v.s. 1.36×10^{16} cm^{-3} for the ZnO(2wt% AuNRs) device and tau (τ) to be 91.2 μs for the ZnO device v.s. 124.9 μs for the ZnO(2wt% AuNRs) device. The higher $n(0)$ value clearly suggests that solar cells with AuNRs can generate more free-carriers after photo-excitation, which is consistent with its higher observed J_{sc}. Prolonged τ also suggests that the photo-generated carriers can survive much longer without recombination in plasmonic devices.

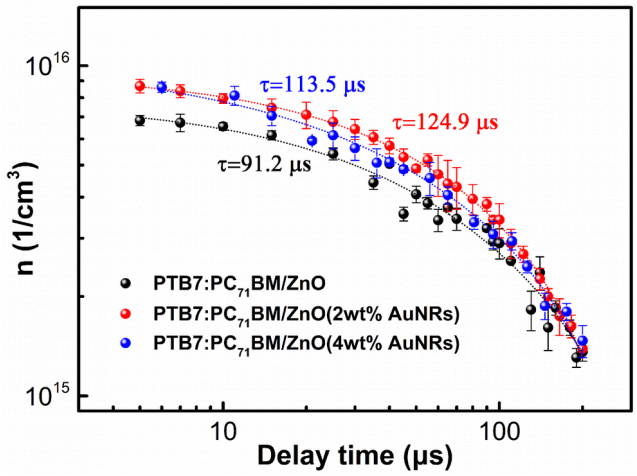

Figure 8. The extracted carrier density as a function of delay time and the fit of discrete points.

One reason to embed anisotropic AuNRs into the ZnO ETL was to encourage trap filling in the ETL and boost its mobility. Another motivation for putting this layer in the cell was to use the longer side of the AuNRs to back-scatter light and enhance light trapping. The higher $n(0)$ derived from photo-CELIV analysis has suggested more efficient photon-to-carrier conversion. Therefore we finally examine how the nanorods changed the optical properties of the devices. Figure 9 depicts the UV-vis absorption of PTB7:PC_{71}BM/ZnO film without and with AuNRs. A small increase in absorption in the region from 500 to 700 nm was observed after depositing ZnO/AuNRs composite film, which reflects some near-field coupling of LSPR into adjacent active layer. It is possible that the plasmons will decay via near field coupling, by performing detailed electromagnetic modeling of the NP and surrounding medium the exact magnitude of each loss path could be identified.[52]

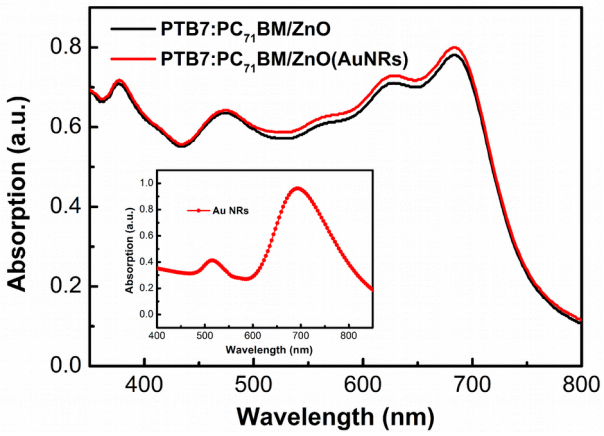

Figure 9. UV-vis absorption spectrum of PTB7:PC_{71}BM/ZnO without and with AuNRs.

The reflection spectra (R) of plasmonic device was also measured and compared with the pure ZnO one, this is shown in Figure 10a. The plasmonic device showed a relatively lower reflectance than the pristine one. The derived absorption spectra (A=1-R)[53] has been plotted in Figure 10b. It can be seen the plasmonic device has enhanced light trapping in a broad range

between 370 to 720 nm. This enhancement is more obvious between 480-580 nm than the other regions, which corresponds to the transverse absorption band from longer side of AuNRs. It is possible that the introduction of the nanorods has changed the refractive index of the ZnO layer, and thus the modal distribution of the light within the device, and this could be the root cause for the increase in light absorption. To rule this out, the complex refractive index of the active layer and the ZnO layers (with and without nanorods) were measured and a transfer matrix model used to calculate the change in the distribution of photons in the device caused by the introduction of the nanorods. It was found that the photon density increased by only 1.4% in the active layer of the plasmonic device, which is not enough to account for the observed optical enhancement (full results in the Supporting Information).

If the EQE spectrum of the device is normalized by the absorption spectrum (IQE=EQE/A) one can calculate the internal quantum efficiency (IQE). This is a measure of how efficient the generation and transport/recombination processes are within the device while excluding changes in absorption between cells.[54] Figure 10b also plots the IQE spectra for both the plasmonic and non-plasmonic device. The plasmonic device shows a significantly higher IQE spectrum than the non-plasmonic device. This further supports our assertion that the main reason for the increase in the device efficiency is due to trap filling.

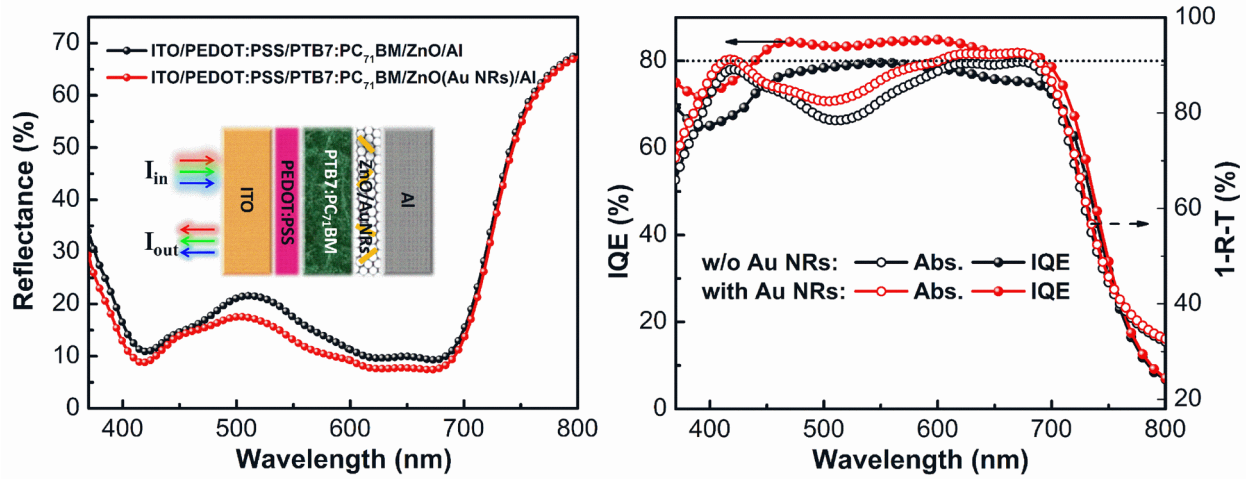

Figure 10. (a): the reflection spectra of two types of devices in reflection geometry; (b): total light absorption (open circles) and IQE (filled circles) curves of the reference and plasmonic devices.

Finally, we use net photocurrent density (J_{ph}) versus effective voltage (V_{eff}) analysis, to estimate the effect AuNRs have on charge generation and charge collection under operating conditions. J_{ph} is calculated as $J_{ph}=J_L-J_D$, in which J_L and J_D are the current density collected under illumination and in the dark, respectively. V_{eff} is determined as $V_{eff}=V_0-V_a$, where V_a is the applied bias voltage and V_0 represents the compensation voltage at which J_{ph} equals zero. The J_{ph}-V_{eff} curves for the devices are shown in Figure 11a. These traces can conceptually be divided into three regions by the maximum power point and short circuit current point. At low V_{eff} region (V_{eff}<0.26 V), J_{ph} is proportional to effective voltage, electric-field dependent carrier drift plays an important role in this region. The higher J_{ph} of plasmonic devices again suggests more efficient charge extraction and collection. Then, as the voltage increased, the rate of increase of J_{ph} becomes slower as field-dependent exciton dissociation starts to dominate. Then J_{ph} get saturated, under these circumstances, exciton dissociation and carrier drift are no longer a

limitation and saturation photocurrent density ($J_{ph,sat}$) is only limited by the charge carrier generation rate (G_{max}).[55] Thus one can write

$$J_{ph,sat} = qG_{max}L$$

in which q is the elementary charge and L is the thickness of active layer (~95 nm in this work). The G_{max} values of the reference and plasmonic device (2wt% AuNRs) are 1.12×10^{28} $m^{-3}s^{-1}$ ($J_{ph,sat}$=170.3 $A\cdot m^{-2}$) and 1.22×10^{28} $m^{-3}s^{-1}$ ($J_{ph,sat}$=184.7 $A\cdot m^{-2}$), respectively. We attribute the noticeably increase in G_{max} to light scattering stems from AuNRs. By normalizing J_{ph} with $J_{ph,sat}$ as shown in Figure 11b, we can estimate charge collection efficiency ($P_{c,m}$) under maximum power conditions and the exciton dissociation efficiency ($P_{c,sc}$) at short circuit condition.[56] The $P_{c,m}$ shows an increase from 75.8% to 82.9% by the introduction of the nanorods, comparing well with the measured improvement in IQE.

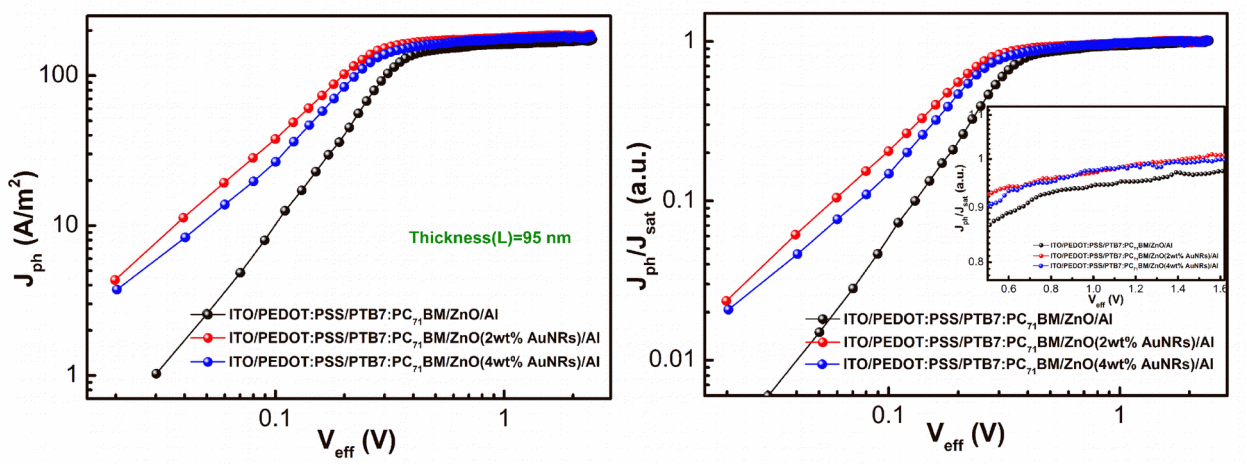

Figure 11. (a): the J_{ph}-V_{eff} characteristics of OSCs without and with AuNRs; (b): normalized J_{ph} with $J_{ph,sat}$ as a function of V_{eff} curves for reference and plasmonic devices.

CONCLUSIONS

In conclusion, we have used a plasmonically functionalized ZnO electron transport layer containing AuNRs to capture photons in the visible region and convert them to hot charge carriers. These hot charge carriers, filled trap states in the ZnO layer, which improved extraction efficiency of the device. This effect is analogous to the light-soaking effect often observed in organic solar cells, but with the advantage of not needing damaging UV light to perform the activation. Solar cell efficiency was eventually raised from 7.91% to 9.36%.

ASSOCIATED CONTENT

Supporting Information

The Supporting Information is available free of charge.

Supplementary experimental details, Figures S1−S7, and additional references (PDF)

AUTHOR INFORMATION

Corresponding Author

*E-mail: sp_wen@jlu.edu.cn.

*E-mail: Roderick.Mackenzie@nottingham.ac.uk

Notes

The authors declare no competing financial interest.

ACKNOWLEDGMENT

This work was supported by the National Natural Science Foundation of China (Grant Nos. 51303061, 11574110), the Project of Science and Technology Development Plan of Jilin

Province (Grant No. 20140204056GX), the Project of Science and Technology Plan of Changchun City (Grant No.13KG49), Opened Fund of the State Key Laboratory on Applied Optics, and the China Postdoctoral Science Foundation (Grant Nos. 2014T70288, 2013M541299).

REFERENCES

(1) Burda, C.; Chen, X. B.; Narayanan, R.; El-Sayed, M. A. Chemistry and properties of nanocrystals of different shapes. *Chemical Reviews* **2005**, *105*, 1025-1102.

(2) Huang, X.; Neretina, S.; El-Sayed, M. A. Gold nanorods: from synthesis and properties to biological and biomedical applications. *Adv. Mater.* **2009**, *21*, 4880-910.

(3) Gan, Q.; Bartoli, F. J.; Kafafi, Z. H. Plasmonic-enhanced organic photovoltaics: breaking the 10% efficiency barrier. *Adv. Mater.* **2013**, *25*, 2385-2396.

(4) Jiang, R.; Chen, H.; Shao, L.; Li, Q.; Wang, J. Unraveling the evolution and nature of the plasmons in (Au core)-(Ag shell) nanorods. *Adv. Mater.* **2012**, *24*, OP200-OP207.

(5) Lu, X.; Rycenga, M.; Skrabalak, S. E.; Wiley, B.; Xia, Y. Chemical synthesis of novel plasmonic nanoparticles. *Annual Review of Physical Chemistry* **2009**, *60*, 167-192.

(6) Hutter, E.; Fendler, J. H. Exploitation of localized surface plasmon resonance. *Adv. Mater.* **2004**, *16*, 1685-1706.

(7) Hou, J.-L.; Fischer, A.; Yang, S.-C.; Benduhn, J.; Widmer, J.; Kasemann, D.; Vandewal, K.; Leo, K. Plasmon-Induced Sub-Bandgap Photodetection with Organic Schottky Diodes. *Adv. Funct.l Mater.* **2016**, *26*, 5741-5747.

(8) Liu, S.; Jiang, R.; You, P.; Zhu, X.; Wang, J.; Yan, F. Au/Ag core–shell nanocuboids for high-efficiency organic solar cells with broadband plasmonic enhancement. *Energy Environ. Sci.* **2016**, *9*, 898-905.

(9) Y. Oh, J. W. Lim, J. G. Kim, H. Wang, B. H. Kang, Y. W. Park, H. Kim, Y. J. Jang, J. Kim, D. H. Kim and B. K. Ju, *ACS Nano*, 2016, **10**, 10143.

(10) Callahan, D. M.; Munday, J. N.; Atwater, H. A. Solar Cell light trapping beyond the ray optic limit. *Nano Lett.* **2012**, *12*, 214-218.

(11) Atwater, H. A.; Polman, A. Plasmonics for improved photovoltaic devices. *Nature Materials* **2010**, *9*, 205-213.

(12) Green, M. A.; Pillai, S. Harnessing plasmonics for solar cells. *Nature Photonics* **2012**, *6*, 130-132.

(13) Y. H. Jang, Y. J. Jang, S. Kim, L. N. Quan, K. Chung and D. H. Kim, *Chem. Rev.*, 2016. DOI: 10.1021/acs.chemrev.6b00302.

(14) Lana-Villarreal, T.; Gómez, R. Tuning the photoelectrochemistry of nanoporous anatase electrodes by modification with gold nanoparticles: Development of cathodic photocurrents. *Chem. Phys. Lett.* **2005**, *414*, 489-494.

(15) Knight, M. W.; Sobhani, H.; Nordlander, P.; Halas, N. J. Photodetection with Active Optical Antennas. *Science* **2011**, *332*, 702-704.

(16) Tian, Y.; Shi, X.; Lu, C.; Wang, X.; Wang, S. Charge separation in solid-state gold nanoparticles-sensitized photovoltaic cell. *Electrochem. Commun.* **2009**, *11*, 1603-1605.

(17) Zhao, G. L.; Kozuka, H.; Yoko, T. Sol-gel preparation and photoelectrochemical properties of TiO2 films containing Au and Ag metal particles. *Thin Solid Films* **1996**, *277*, 147-154.

(18) Tian, Y.; Tatsuma, T. Mechanisms and Applications of Plasmon-Induced Charge Separation at TiO2 Films Loaded with Gold Nanoparticles. *J. Am. Chem. Soc.* **2005**, *127*, 7632-7637.

(19) Kawahara, K.; Suzuki, K.; Ohko, Y.; Tatsuma, T. Electron transport in silver-semiconductor nanocomposite films exhibiting multicolor photochromism. *Phys. Chem. Chem. Phys. : PCCP* **2005**, *7*, 3851-3855.

(20) Furube, A.; Du, L.; Hara, K.; Katoh, R.; Tachiya, M. Ultrafast plasmon-induced electron transfer from gold nanodots into TiO2 nanoparticles. *J. Am. Chem. Soc.* **2007**, *129*, 14852-14853.

(21) Chen, H. M.; Chen, C. K.; Chen, C. J.; Cheng, L. C.; Wu, P. C.; Cheng, B. H.; Ho, Y. Z.; Tseng, M. L.; Hsu, Y. Y.; Chan, T. S.; Lee, J. F.; Liu, R. S.; Tsai, D. P. Plasmon Inducing Effects for Enhanced Photoelectrochemical Water Splitting: X-ray Absorption Approach to Electronic Structures. *ACS Nano* **2012**, *6*, 7362-7372.

(22) Sun, Y.; Seo, J. H.; Takacs, C. J.; Seifter, J.; Heeger, A. J. Inverted polymer solar cells integrated with a low-temperature-annealed sol-gel-derived ZnO Film as an electron transport layer. *Adv. Mater.* **2011**, *23*, 1679-1683.

(23) Wen, S.; Wang, C.; Ma, P.; Wang, G.; Dong, W.; Gao, Y.; Ruan, S. Improved Efficiency in Dithieno[3,2-b:2′,3′-d]silole-Based Polymer Solar Cells by the Insertion of ZnO Optical Spacer. *J. Phys. Chem. C* **2015**, *119*, 20817-20822.

(24) Ischenko, V.; Polarz, S.; Grote, D.; Stavarache, V.; Fink, K.; Driess, M. Zinc oxide nanoparticles with defects. *Adv. Funct.l Mater.* **2005**, *15*, 1945-1954.

(25) Small, C. E.; Chen, S.; Subbiah, J.; Amb, C. M.; Tsang, S.-W.; Lai, T.-H.; Reynolds, J. R.; So, F. High-efficiency inverted dithienogermole–thienopyrrolodione-based polymer solar cells. *Nature Photonics* **2011**, *6*, 115-120.

(26) Trost, S.; Zilberberg, K.; Behrendt, A.; Polywka, A.; Görrn, P.; Reckers, P.; Maibach, J.; Mayer, T.; Riedl, T. Overcoming the "Light-Soaking" Issue in Inverted Organic Solar Cells by the Use of Al:ZnO Electron Extraction Layers. *Adv. Energy Mater.* **2013**, *3*, 1437-1444.

(27) Ecker, B.; Egelhaaf, H.-J.; Steim, R.; Parisi, J.; von Hauff, E. Understanding S-Shaped Current–Voltage Characteristics in Organic Solar Cells Containing a TiOx Interlayer with Impedance Spectroscopy and Equivalent Circuit Analysis. *J Phys. Chem. C* **2012**, *116*, 16333-16337.

(28) Zhou, Y.; Shim, J. W.; Fuentes-Hernandez, C.; Sharma, A.; Knauer, K. A.; Giordano, A. J.; Marder, S. R.; Kippelen, B. Direct correlation between work function of indium-tin-oxide electrodes and solar cell performance influenced by ultraviolet irradiation and air exposure. *Phys. Chem. Chem. Phys. : PCCP* **2012**, *14*, 12014-12021.

(29) Chen, S.; Small, C. E.; Amb, C. M.; Subbiah, J.; Lai, T.-h.; Tsang, S.-W.; Manders, J. R.; Reynolds, J. R.; So, F. Inverted Polymer Solar Cells with Reduced Interface Recombination. *Adv.Energy Mater.* **2012**, *2*, 1333-1337.

(30) Jorgensen, M.; Norrman, K.; Gevorgyan, S. A.; Tromholt, T.; Andreasen, B.; Krebs, F. C. Stability of polymer solar cells. *Adv. Mater.* **2012**, *24*, 580-612.

(31) Zhang, D.; Choy, W. C. H.; Xie, F.; Sha, W. E. I.; Li, X.; Ding, B.; Zhang, K.; Huang, F.; Cao, Y. Plasmonic Electrically Functionalized TiO2f or High-Performance Organic Solar Cells. *Adv. Funct. Mater.* **2013**, *23*, 4255-4261.

(32) Govorov, A. O.; Zhang, H.; Demir, H. V.; Gun'ko, Y. K. Photogeneration of hot plasmonic electrons with metal nanocrystals: Quantum description and potential applications. *Nano Today* **2014**, *9*, 85-101.

(33) D. D. Evanoff, Jr. and G. Chumanov, *Chemphyschem*, 2005, **6**, 1221.

(34) K. Yu, Y. Tian and T. Tatsuma, *Phys. Chem. Chem. Phys.*, 2006, **8**, 5417.

(35) V. Jankovic, Y. Yang, Jz. You, L. Dou, Y. Liu, P. Cheung, J. P. Chang and Y. Yang, *ACS Nano*, 2013, **7**, 3815.

(36) E. Kazuma, N. Sakai and T. Tatsuma, *Chem. Commun.*, 2011, **47**, 5777.

(37) A. Pescaglini, A. Martin, D. Cammi, G. Juska, C. Ronning, E. Pelucchi and D. Iacopino, *Nano Lett.*, 2014, **14**, 6202.

(38) C. Clavero, *Nat. Photon.*, 2014, **8**, 95.

(39) S. Linic, P. Christopher and D. B. Ingram, *Nat. Mater.*, 2011, **10**, 911.

(40) Liao, Z.-M.; Zhang, H.-Z.; Zhou, Y.-B.; Xu, J.; Zhang, J.-M.; Yu, D.-P. Surface effects on photoluminescence of single ZnO nanowires. *Phys. Lett. A* **2008**, *372*, 4505-4509.

(41) Dkhil, S. B.; Duché, D.; Gaceur, M.; Thakur, A. K.; Aboura, F. B.; Escoubas, L.; Simon, J.-J.; Guerrero, A.; Bisquert, J.; Garcia-Belmonte, G.; Bao, Q.; Fahlman, M.; Videlot-Ackermann, C.; Margeat, O.; Ackermann, J. Interplay of Optical, Morphological, and Electronic Effects of ZnO Optical Spacers in Highly Efficient Polymer Solar Cells. *Adv. Energy Mater.* **2014**, 1400805.

(42) Lu, L.; Luo, Z.; Xu, T.; Yu, L. Cooperative plasmonic effect of Ag and Au nanoparticles on enhancing performance of polymer solar cells. *Nano Lett.* **2013**, *13*, 59-64.

(43) Liu, S.; You, P.; Li, J.; Li, J.; Lee, C.-S.; Ong, B. S.; Surya, C.; Yan, F. Enhanced efficiency of polymer solar cells by adding a high-mobility conjugated polymer. *Energy Environ. Sci.* **2015**, *8*, 1463-1470.

(44) Zhang, W.; Wu, Y.; Bao, Q.; Gao, F.; Fang, J. Morphological Control for Highly Efficient Inverted Polymer Solar Cells Via the Backbone Design of Cathode Interlayer Materials. *Adv. Energy Mater.* **2014**, *4*, 1400359.

(45) B. Wu, X. Wu, C. Guan, K. Fai Tai, E. K. Yeow, H. Jin Fan, N. Mathews and T. C. Sum, *Nat. Commun.*, 2013, **4**, 2004.

(46) Liang, Y.; Xu, Z.; Xia, J.; Tsai, S. T.; Wu, Y.; Li, G.; Ray, C.; Yu, L. For the bright future-bulk heterojunction polymer solar cells with power conversion efficiency of 7.4%. *Adv. Mater.* **2010**, *22*, E135-E138.

(47) Guo, X.; Zhang, M.; Tan, J.; Zhang, S.; Huo, L.; Hu, W.; Li, Y.; Hou, J. Influence of D/A ratio on photovoltaic performance of a highly efficient polymer solar cell system. *Adv. Mater.* **2012**, *24*, 6536-6541.

(48) MacKenzie, R. C. I.; Shuttle, C. G.; Dibb, G. F.; Treat, N.; von Hauff, E.; Robb, M. J.; Hawker, C. J.; Chabinyc, M. L.; Nelson, J. Interpreting the Density of States Extracted from Organic Solar Cells Using Transient Photocurrent Measurements. *J. Phys. Chem. C* **2013**, *117*, 12407-12414.

(49) Hanfland, R.; Fischer, M. A.; Brutting, W.; Wurfel, U.; MacKenzie, R. C. I. The physical meaning of charge extraction by linearly increasing voltage transients from organic solar cells. *Appl.Phys. Lett.* **2013**, *103*, 063904.

(50) T. M. Clarke, C. Lungenschmied, J. Peet, N. Drolet and A. J. Mozer, *Adv. Energy Mater.*, 2015, **5**, 1401345.

(51) Clarke, T. M.; Peet, J.; Denk, P.; Dennler, G.; Lungenschmied, C.; Mozer, A. J. Non-Langevin bimolecular recombination in a silole-based polymer:PCBM solar cell measured by time-resolved charge extraction and resistance-dependent time-of-flight techniques. *Energy Environ. Sci.* **2012**, *5*, 5241-5245.

(52) N. Lagos, M. M. Sigalas and E. Lidorikis, *Appl. Phys. Lett.*, 2011, **99**, 063304.

(53) Li, X.; Choy, W. C.; Huo, L.; Xie, F.; Sha, W. E.; Ding, B.; Guo, X.; Li, Y.; Hou, J.; You, J.; Yang, Y. Dual plasmonic nanostructures for high performance inverted organic solar cells. *Adv. Mater.* **2012**, *24*, 3046-3052.

(54) Park, S. H.; Roy, A.; Beaupré, S.; Cho, S.; Coates, N.; Moon, J. S.; Moses, D.; Leclerc, M.; Lee, K.; Heeger, A. J. Bulk heterojunction solar cells with internal quantum efficiency approaching 100%. *Nature Photonics* **2009**, *3*, 297-302.

(55) He, Z.; Zhong, C.; Huang, X.; Wong, W. Y.; Wu, H.; Chen, L.; Su, S.; Cao, Y. Simultaneous enhancement of open-circuit voltage, short-circuit current density, and fill factor in polymer solar cells. *Adv. Mater.* **2011**, *23*, 4636-4643.

(56) Long, G.; Wan, X.; Kan, B.; Hu, Z.; Yang, X.; Zhang, Y.; Zhang, M.; Wu, H.; Huang, F.; Su, S.; Cao, Y.; Chen, Y. Impact of the electron-transport layer on the performance of solution-processed small-molecule organic solar cells. *ChemSusChem* **2014**, *7*, 2358-2364.